

# Reducing the CO<sub>2</sub> footprint at an LNG asset with replicate trains using operational data-driven analysis. A case study on end flash vessels.

Rakesh Paleja<sup>a</sup>, Osemwinyen Ekhotorumwen<sup>b</sup>, Matthew Jones<sup>c</sup>, John Ayoola<sup>b</sup>, Raghuraman Pitchumani<sup>d</sup>, Philip Jonathan<sup>a,e</sup>

<sup>a</sup>*Shell Research Limited, London, United Kingdom.*

<sup>b</sup>*NLNG Plant Complex, Bonny Island, Rivers State, Nigeria*

<sup>c</sup>*Shell Global Solutions International BV, Amsterdam, The Netherlands.*

<sup>d</sup>*Shell International Exploration and Production Inc., Houston, Texas, USA.*

<sup>e</sup>*Department of Mathematics and Statistics, Lancaster University, United Kingdom.*

---

## Abstract

A liquefied natural gas (LNG) facility often incorporates replicate liquefaction trains. The performance of equivalent units across trains, designed using common numerical models, might be expected to be similar. In this paper, we discuss statistical analysis of real plant data to validate this assumption. Analysis of operational data for end flash vessels from a pair of replicate trains at an LNG facility indicates that one train produces 2.8% to 6.4% more end flash gas than the other. We then develop statistical models for train operation, facilitating reduced flaring and hence a reduction of up to 45% in CO<sub>2</sub> equivalent flaring emissions, noting that flaring emissions for a typical LNG facility account for approximately 4% to 8% of the overall facility emissions. We recommend that operational data-driven models be considered generally to improve the performance of LNG facilities and reduce their CO<sub>2</sub> footprint, particularly when replica units are present.

---

## 1. Introduction

Natural gas (NG) plays a significant role in the global energy transition, since switching from coal to NG reduces greenhouse gas emissions by 50% when producing electricity and 33% when providing heat; globally, up to 500 MtCO<sub>2</sub> were avoided in 2018 compared to 2010 (International Energy Agency, 2019). Natural gas sources in Australia, the Middle East, Russia, North America and Africa are often distant from consumer demand in Europe, Japan, South Korea, China and developing Asia (International Energy Agency, 2022). Transporting natural gas via pipeline over distances > 3000 km is not economically viable due to the low energy density of natural gas on a volumetric basis. Liquefaction of NG to -163°C reduces its volume by a factor of around 600, permitting transportation by sea (Hafner and Luciani, 2022).

A large-scale LNG train typically consumes 14.3 kW/tonne/day of LNG, with 40-60% of the energy used by compressors (Hasan et al., 2009a). The energy required is normally provided by fuel gas (FG) generated from different sources at the LNG producing facility including end flash gas (EFG) from end flash vessels, and boil off gas (BOG) from storage tanks and from loading vessels (LBOG). Economically and environmentally, it is advantageous to reduce demand for FG as much as possible consistent with demand, whilst avoiding flaring of excess FG. This is achieved by process modelling using software such as AspenTech's HYSYS®, UniSim® and MATLAB®. These software packages use numerical algorithms as summarised e.g. by Bassioni and Klein (2024) and Austbo et al. (2014).

For example on the demand side, in Alabdulkarem et al. (2011), minimization of the power of the compressor (which consumes FG) in a C3MR process is performed through simulation in Aspen HYSYS® and optimization in MATLAB® using a genetic algorithm, leading to a 9% reduction in energy requirement. Further, Jackson et al. (2017) optimises the energy requirement for a typical LNG train at different geographical locations using numerical methods and concludes that liquefaction in colder climates such as that of Norway would require 20-26% lower energy compared to warmer Australian or Middle Eastern climates. Thus a given compressor can provide more LNG in colder countries. In Ali et al. (2018), FG demand for a single mixed refrigerant liquefaction process is optimised using the meta-heuristic vortex search algorithm; optimal values of mixed refrigerant flow rates and process operating pressures are determined in the vortex pattern corresponding to the minimum required energy, which is reduced by 41.5%. In Castillo et al. (2013), options to pre-cool NG are studied for hot and cold climate conditions using HYSYS® to determine the most energy efficient technology for either climate.

On the supply side, in Hasan et al. (2009b), dynamic simulations are conducted to facilitate reducing in LBOG using "heel" as a parameter to be optimised; heel is the amount of LNG that is retained in the LNG vessel during its return

journey to maintain the vessel as close as possible to -163 °C. Numerical simulation studies have been developed by Kurle et al. (2017) for LBOG involving variables such as heat leak, initial-temperature of LNG ship-tank, compressor capacity, and maximum cooling-rate for ship-tank in the model. The study is expected to help proper handling of BOG problems in terms of minimizing flaring at LNG exporting terminals, and thus reducing waste, saving energy. Numerical simulations by Jin et al. (2023) on BOG generation and recovery at LNG exporting terminals have been carried out to understand the Specific Energy Consumption (SEC) using single mixed refrigerant and compare it with a typical Mark III process. The proposed SMR design has 50.34% lower SEC than a Mark III process. Shin et al. (2022) models excessive BOG generated due to the temperature difference between the LNG and a tank and designs a model predictive control (MPC) system to simultaneously regulate the pressure and temperature of the tank by manipulating the vapour outlet flow rate and the amount of LNG spray injected during the cool-down process. In Widodo and Muharam (2023), simulation models for BOG generation during liquefaction and loading processes are discussed for a typical LNG production plant producing 8 million tonnes/year LNG, limited by capacity of BOG recovery. Numerical optimisation shows a potential production increase from BOG recovery and fuel gas optimization to be around 90,260 tonnes/ year or equivalent to 1.4 cargo of LNG per year. A numerical simulation of the flow of LNG stored in a small-sized cylindrical tank is presented in Ferrin and Perez-Perez (2020). The work suggests that the filling level of the tank substantially influences the boiling rate and the degree of stratification, as well as the flow structures generated by free convection.

We note that alternative numerical methods exists to model BOG generated during shipping of LNG. For instance, in Wu and Ju (2021), the BOG generation characteristics in a type C independent liquefied natural gas (LNG) tank under sloshing excitation are studied using computational fluid dynamics (CFD). Results show that sloshing excitation influences the thermo-physical process and BOG generation of the LNG tank. Such numerical studies do not consider the facts that BOG generation from the LNG tank, and LBOG can vary significantly due to climatic conditions, the nature and size of the loading vessels and other factors. Further, we are not aware of literature that considers the varying nature of real-time FG supply (from multiple suppliers) and demand.

Moreover, the literature addressing the use of real operational plant data for process optimisation is limited. Katebah et al. (2023) note the considerable potential for, yet the dearth of literature on, the exploitation of real plant data to optimise the performance of LNG processes, over and above that achieved using numerical simulation.

Typically, multiple trains at a given LNG production facility have the same design. Multiple trains are preferred over a single large train for reasons such as (a) improved robustness of production to interruptions on an individual train, and (b) physical limitations on the design of a single large train. When multiple trains are operated at an actual LNG facility, some trains may be exact replicas of others in terms of liquefaction technology, size of compressors and other units such as end flash vessels. Yet the literature examining the performance of multiple trains, from a numerical or operation plant data perspective, is again limited.

### *Objectives and layout*

In this paper, we use a two-step data-driven approach to demonstrate divergence in performance between two replicate trains at a full-scale LNG facility, focusing on comparison of end flash vessels at an LNG facility. We emphasise that this paper exploits real operational data from the full-scale LNG facility. The first analysis step (reported in Section 3.1) involves exploratory analysis of historical data corresponding to multiple years of operation, to elucidate whether flash vessels from different trains produce different amounts of EFG under similar process conditions. Then we use statistical hypothesis testing (Section 3.2) to confirm significant divergence in EFG production between LNG trains. The second step (Section 3.3) involves the estimation of regression models for EFG production with respect to driver manipulable process variables. We demonstrate (Section 3.4) that these can be used to control excess EFG to minimise excess end flash gas and reduce CO<sub>2</sub> footprint. We emphasise that the two-step approach is not specific to any particular process unit or production technology. All that is required is a representative period of historical operational data for the near-replica production units.

Preceding the main analysis sections, Section 2 provides an overview of typical large-scale liquefaction. Following the analysis, Section 4 then provides discussion and conclusions. Summary statistics for flow rate from the two end flash vessels considered, and details of statistical hypothesis testing using Welch's t-test are relegated to Appendices A and B.

## **2. Description of LNG process**

This section provides a brief overview of the components and operation of a liquefaction train, followed by a discussion of LNG facilities containing replicate trains and the potential this offers for improved operation.

## 2.1. The liquefaction train

A liquefaction train at an LNG facility is comprised of a hot and a cold section. NG from the gas field enters hot section, operating at above ambient temperature. Here, NG is pre-treated to remove acid gas (carbon dioxide and hydrogen sulphide), water and mercury. The processed NG then enters the cold section at temperature T1, pressure P1 and flow rate Q1 respectively as shown in Figure 1. Temperature T1 depends on the geographical location and

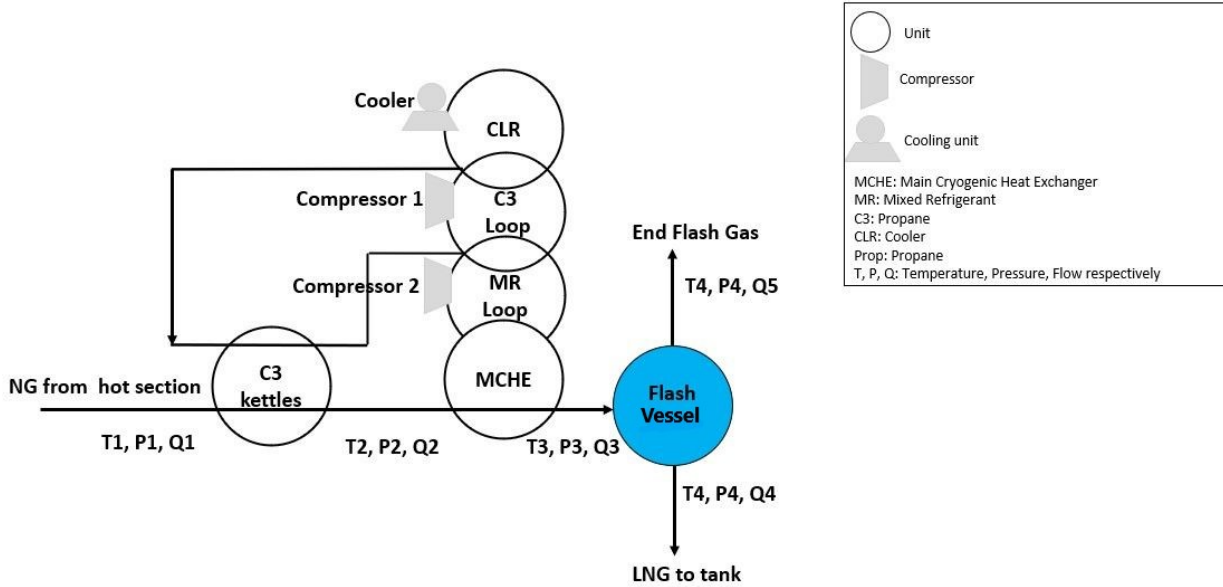


Figure 1: Schematic of cold section of LNG train. The end flash vessel shown in blue produces end flash gas, used as fuel gas for the facility

can vary from 25 to 30 °C, pressure P1 usually ranges from 50 to 60 bar whereas mass flow rate Q1 (Tonnes per day, T/d) depends on the availability of NG. There are different designs for the cold section. In the C3MR design (Lim et al., 2012), the cold section pre-cools NG in C3 kettles from T1 to temperature T2 and subsequently to T3 in the main cryogenic heat exchanger (MCHE) using a mixed refrigerant (MR). MR consists of nitrogen (N<sub>2</sub>), C1, C2 and C3. T2 usually approaches -30 to -27 °C whereas T3 ranges from -150 to -145 °C depending on a variety of factors such as NG composition, MR composition and pressure, and flow rates of NG and MR. The C3 kettles and MCHE are shell-and-tube heat exchanger units with NG flowing on the tube side, C3 in the kettles and MR in the MCHE, both on the shell side. The duty required to circulate propane and MR to cool NG from T1 to T3 is provided by two compressors. Figure 1 illustrates compressor 1 (C3) and compressor 2 (MR). Cooling NG from T1 to T3 results in vaporisation of C3 and MR; vapour heat is ejected to the atmosphere by air or water cooler before returning back to C3 kettles and MCHE respectively. When upstream pressure P1 is high, the final cooling to T4= -163°C occurs in the flash vessel, where NG from MCHE is flash evaporated at pressure P4 (close to the atmospheric pressure). As a result, the flow Q3 from the MCHE is divided into a vapour stream with flow rate Q5, and a liquid stream with flow rate Q4, the latter to storage tanks maintained at atmospheric pressure. The vapour stream is EFG to the FG pool, whereas the liquid stream is LNG for export. The nature of the flash evaporation process is such that Q5 ≪ Q4 with Q3 = Q4 + Q5 to retain mass balance; the temperatures and pressures of the EFG and LNG are similar.

## 2.2. Replicate trains

As noted in Section 1, LNG facilities often contain replicate trains; Figure 2 shows a schematic for two replicate trains studied in this paper. Here, EFG from end flash vessels of each train is sent to the FG pool along with other sources of FG such as BOG and LBOG. The FG pool supplies the FG to the LNG facility. When there is excess FG, the flare valve is opened and the excess FG is flared. To prevent flaring, typical practice is to reduce EFG production from both trains equally, since trains are notionally replicates by design.

In this work we take advantage of replicate flash vessels at the LNG facility to minimise flare value opening. The presence of replicate components such as compressors, MCHEs, coolers and C3 kettles at LNG facilities generally can be similarly exploited for operational improvements.

## 3. Exploratory data analysis and hypothesis testing

In this section we present an analysis of operational data from an LNG facility with two replicate liquefaction trains. The objective of the analysis is to identify differences in the operating characteristics of the end flash vessels of

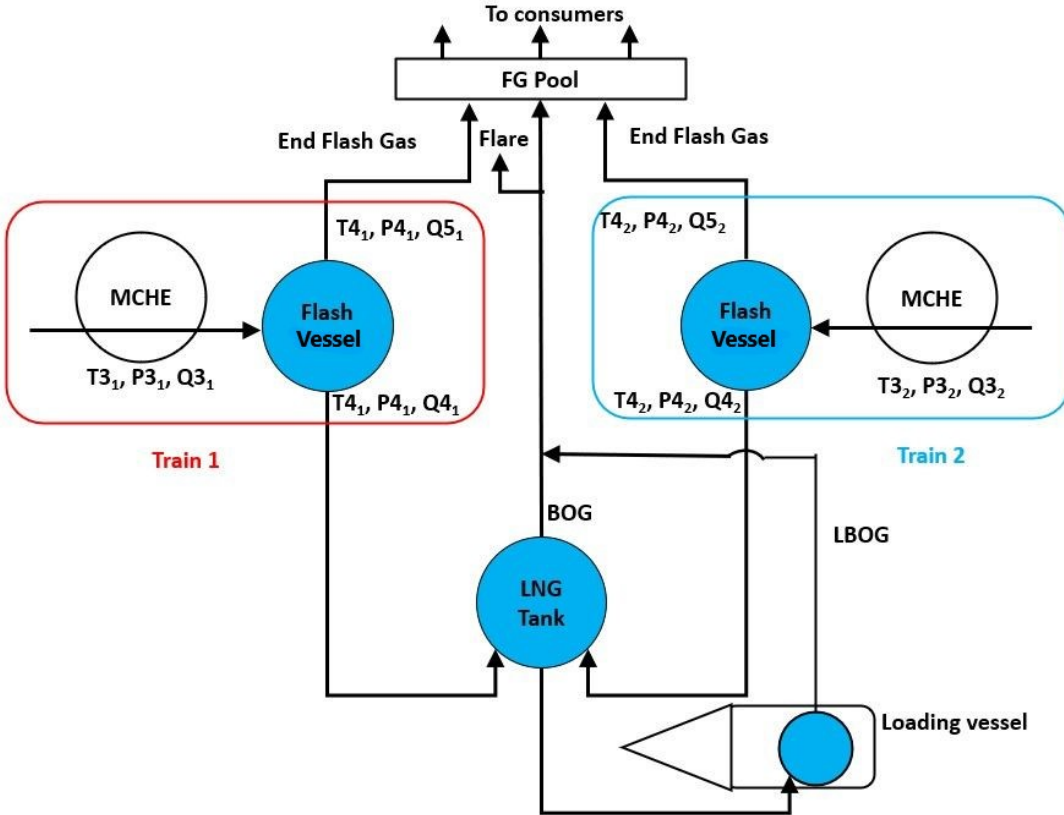


Figure 2: Schematic of two replicate trains, Train 1 and Train 2, feeding EFG to FG pool besides BOG from LNG tank LBOB from tank in the loading vessel (also shown in blue). When the FG pool has excess FG it is released and flared through the flare valve

the two trains. The differences identified are then exploited in Sections 3.3 and 3.4 to improve the overall performance of liquefaction, in particular with respect to reduced flaring of EFG. Section 3.1 provides an exploratory analysis of operational data, and Section 3.2 uses statistical hypothesis testing to demonstrate significant differences in operating characteristics for the trains.

We emphasise that the analysis is intended to exploit different operating characteristics of notionally replicate LNG trains. A necessary preliminary step therefore is to ensure that trains considered are indeed replicates. We have confirmed this for a pair of trains, henceforth identified as  $\text{Tr}_1$  and  $\text{Tr}_2$ , from the LNG facility.

### 3.1. Exploratory analysis

We consider the operation of flash vessel units  $U_1, U_2$  of replicate trains  $\text{Tr}_1, \text{Tr}_2$ , with EFG mass flow rates  $Q_{51}, Q_{52}$ . Figure 1 motivates the assumption that  $Q_5$  for individual units is dependent on (a) the corresponding flow  $Q_3$  of NG from the MCHE to the flash vessel, (b) the outlet temperature  $T_3$  of NG from the MCHE to the flash vessel, and (c) flash vessel pressure  $P_4$ . The “manipulated” (or, in statistical terminology, “treatment”) variables  $Q_3, T_3, P_4$  can be changed independently, thereby influencing  $Q_5$ . We anticipate that increasing the values of  $Q_3$  and  $T_3$  will lead to a higher value of  $Q_5$ . Conversely a higher  $P_4$  will lead to lower  $Q_5$ .

We seek to assess fairly whether  $Q_5$  from  $U_1$  and  $U_2$  is similar. Ideally, we would conduct a series of experiments on both units, where the values of  $Q_3, T_3$  and  $P_4$  were set at common values across trains, and differences in  $Q_5$  quantified. However, such experiments are impractical economically for trains in continuous operation. Nevertheless, over the course of normal operation of the trains in time, the set points of  $Q_3, T_3$  and  $P_4$  for the two trains vary, exploring a domain of typical set points for both trains. We can therefore exploit these historical data to quantify differences in  $Q_5$ . It is of course critical that our assessment is fair, in particular because the domains of  $Q_3, T_3$  and  $P_4$  might be different for the two trains. Since  $Q_5$  depends on  $Q_3, T_3$  and  $P_4$ , it is essential that the historical data for both the trains is filtered such that the treatment variables  $Q_3, T_3$  and  $P_4$  correspond to similar sets of values across the two units. Concisely in mathematical notation, we wish to compare  $Q_5|(Q_3, T_3, P_4)$  conditionally across trains, rather than  $Q_5$  marginally. The simple filter condition applied takes the form

$$\text{LL} \leq X_1^t / X_2^t \leq \text{UL} \quad \text{for all of } X = Q_3, T_3, P_4 \quad (1)$$

where  $X^t$  is the value of  $X$  and time  $t$ , for data sampled every 5 minutes for a period of a contiguous calendar year. We emphasise that the filter considered is applied to all of  $X = Q3, T3$  and  $P4$ . Further, LL indicates a common lower limit for the ratio of manipulated variables across trains, set at 0.98 in this work. UL indicates the corresponding common upper limit, set at 1.02. The effect of filtering manipulated variables is illustrated in Figure 3, for data corresponding to the calendar year 2019. Panels of the figure are scatter plots of  $X_2$  on  $X_1$  for  $X = Q3, T3, P4$  and  $Q5$ , with green dots indicating data for time points at which the filter conditions in Equation 1 are satisfied, corresponding to approximately 10% of the unfiltered sample, over all years of available data. Data for all other time points is shown in blue. Of course, filtering yields subsets of operational data for  $Tr_1$  and  $Tr_2$  of equal size. For reasons of commercial confidentiality, note also that all flows  $Q3$  and  $Q5$  presented in this work (e.g. in Figure 3, Figure 4 and accompanying tables in Appendix A) have been normalised using a common factor  $k$  (i.e. Normalised Flow =  $k \times$  Observed Flow) such that the maximum  $Q5$  (over all trains and years) in the filtered data is 100 T/d after normalisation. No other variables are normalised.

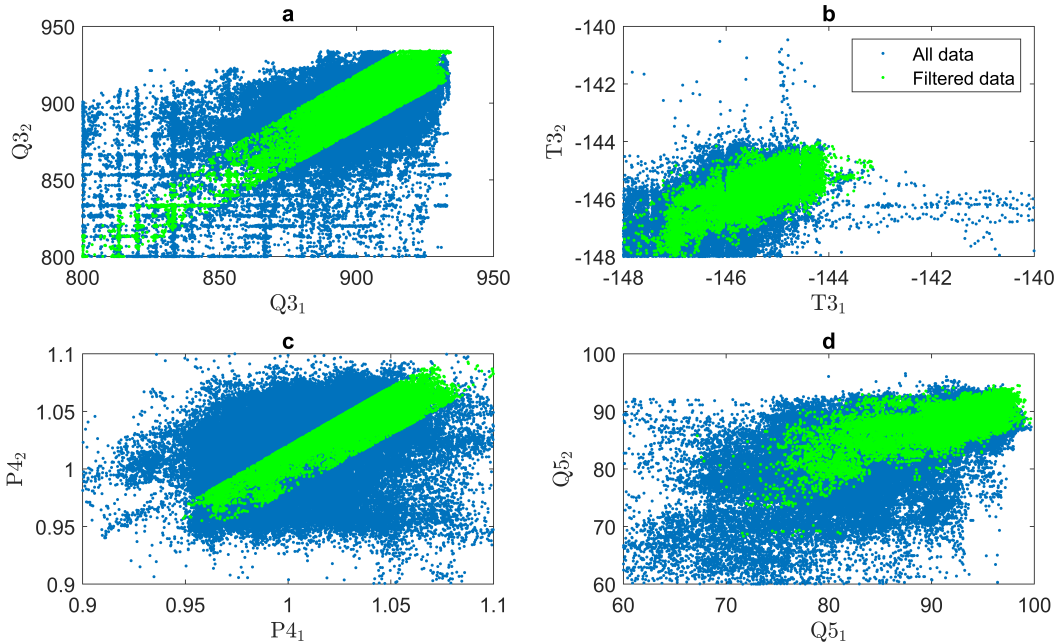


Figure 3: Scatter plots of  $Q3, T3, P4$  and  $Q5$  across trains  $Tr_1, Tr_2$  of operational data sampled at 5 minute intervals for the year 2019. Values for time points satisfying the filter conditions in Equation 1 are shown in green. All other time points are shown in blue. Values of  $Q3$  and  $Q5$  have been normalised using a common factor so that the global maximum value of  $Q5$  is 100 T/d

The quality of NG sourced from upstream wells, distributed to the two trains, varies over time. As the proportion of low boiling point components (e.g. C2, C3, and butane, C4) in NG increases,  $Q5$  production reduces in both  $U_1$  ad  $U_2$ . Moreover, the performance of LNG trains often exhibits seasonal patterns that can influence  $Q5$ ; filtering (Equation 1) ensures that the comparison of units is not influenced by season and other external variation of the common NG input to liquefaction. Filtering therefore allows us to characterise underlying differences in the operational characteristics of the trains, rather than differences in inputs and operating set points.

Since (replicate) trains are optimised through numerical simulations during design, we expect differences in  $Q5$  across trains to be small. We might therefore expect that a comparatively long period of historical data might be required to quantify differences in operational characteristics with confidence: in particular, analysis of filtered data from only one year can lead to spurious conclusions. Therefore here, we analyse historical operational data for the five year period 2015 to 2019. The panels of Figure 4 shows histograms of filtered  $Q5$  per annum for years 2015 to 2019, for train  $Tr_1$  (blue) and  $Tr_2$  (red). The title of each plot shows the year and number  $n$  of filtered 5-minute observations. Vertical blue and red lines and annotated text give sample means of filtered  $Q5_1$  and  $Q5_2$  respectively. Figure 4 suggests for each of the five years, that  $Q5$  through  $U_1$  is greater than that through  $U_2$ . The difference in sample means ranges from 2.5 to 5.5 T/d. Corresponding tables of summary statistics are provided in Appendix A. It is also interesting that the number of observations retained after filtering is considerably higher in 2018 and 2019 than in 2016 in particular, possibly indicating more consistent setting of operational conditions across trains in more recent years.

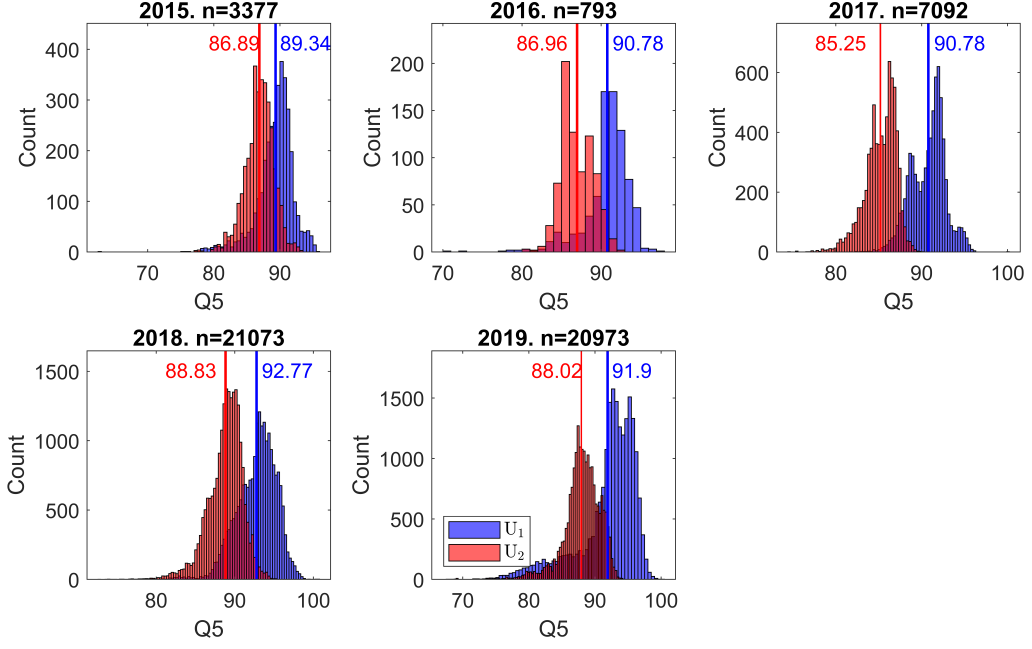


Figure 4: Histograms of filtered  $Q_{51}$  (blue) and  $Q_{52}$  (red) data per annum, for years 2015 to 2019. Panel titles indicate the number of observations  $n$  retained after filtering. Vertical lines and annotated text give mean values of filtered data. Values of  $Q_5$  have been normalised using a common factor so that the global maximum value is 100 T/d

The figure for unfiltered data corresponding to Figure 4 is show in Figure 5. It is notably difficult to see from the figure that there is a material difference between the operating characteristics of trains  $Tr_1$  and  $Tr_2$ . This emphasises the need to consider the conditional behaviour of  $Q_5$  given its driver variables  $Q_3$ ,  $T_3$ ,  $P_4$ .

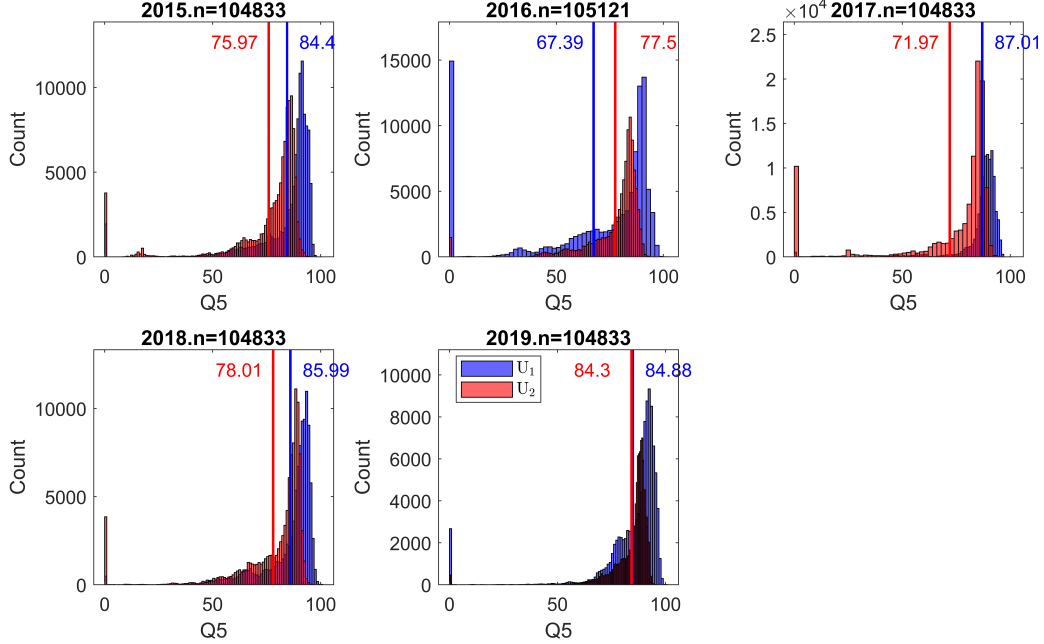


Figure 5: Histograms of full unfiltered data for  $Q_{51}$  (blue) and  $Q_{52}$  (red) per annum, for years 2015 to 2019. Panel titles indicate the number of observations  $n$  retained after filtering. Vertical lines and annotated text give mean values of filtered data. Values of  $Q_5$  have been normalised using a common factor so that the global maximum value is 100 T/d

### 3.2. Statistical testing

The exploratory analysis above suggests that Q5 from vessel U<sub>1</sub> in train Tr<sub>1</sub> is higher than that from U<sub>2</sub> in train Tr<sub>2</sub>. We can quantify this using a statistical hypothesis test to assess whether the population mean  $\bar{Q5}_1$  of Q5 in train Tr<sub>1</sub> is greater than the corresponding population mean  $\bar{Q5}_2$  in train Tr<sub>2</sub>. To perform this one-sided hypothesis test, we set the null hypothesis H<sub>0</sub> that there is no difference between  $\bar{Q5}_1$  and  $\bar{Q5}_2$ , and an alternative hypothesis H<sub>1</sub> that  $\bar{Q5}_1 > \bar{Q5}_2$ . Then we calculate whether there is sufficient evidence in the data to reject the null hypothesis in favour of the alternative. Various parametric and non parametric tests are suggested in the literature (e.g. Marshall and Jonker 2011) for this purpose. The choice of test depends on the nature of the data and the specific question at hand. Here we use the independent two-sample Student's t-test, calculating test-statistic  $t$  measuring the difference in population means relative to the variability within the groups using sample data. This test assumes that the variances of the two samples are approximately equal. For samples of random variables  $X_1$  and  $X_2$  with common sample size  $n$ ,  $t$  is calculated as

$$t = (\bar{X}_1 - \bar{X}_2)/s_d \quad (2)$$

where  $\bar{X}_1$  and  $\bar{X}_2$  are the sample means for Q5<sub>1</sub> and Q5<sub>2</sub> (from Tables A1 and A2 in Appendix A), and  $s_d$  is the standard error of the difference in means given by  $s_d^2 = (s_1^2 + s_2^2)/n$ , where  $s_1^2$  and  $s_2^2$  are corrected sample estimates for the variance of  $X_1$  and  $X_2$ .  $s_d$  can also be written as  $s_d^2 = 2s_p^2/n$ , where  $s_p$  is an estimate for the pooled standard deviation of the samples given by  $s_p^2 = (s_1^2 + s_2^2)/2$ . The test statistic  $t$  follows a t-distribution with  $\nu = 2(n - 1)$  degrees of freedom (Evans et al., 2000). This probability distribution generalizes the standard normal distribution: both the t-distribution and standard normal distribution have mean zero and exhibit a bell-shaped curve, but the t-distribution has heavier tails controlled by shape parameter  $\nu$ . Typically, the null hypothesis H<sub>0</sub> is rejected at the  $\alpha = 0.05$  level; this occurs when the value of the t-statistic calculated exceeds a critical value  $t_{\text{crit},\nu}(1 - \alpha)$  equal to the  $(1 - \alpha) \times 100 = 95\%$ ile of the t-distribution with  $\nu$  degrees of freedom.

$$(\bar{X}_1 - \bar{X}_2)/s_d - t_{\text{crit},\nu}(0.95) > 0. \quad (3)$$

Multiplying the left hand side above by  $s_d$  gives  $(\bar{X}_1 - \bar{X}_2) - s_d \times t_{\text{crit},\nu}(0.95)$ , equal to the lower confidence limit LCL for the difference  $\bar{X}_1 - \bar{X}_2$  in population means. Rejecting H<sub>0</sub> is therefore also equivalent to estimating LCL<sub>0</sub>. For total sample  $n > 100$ ,  $t_{\text{crit},2(n-1)}(0.95) \approx 1.645$ , the 95%ile of standard normal distribution, to at least two decimal places; for smaller sample sizes, values of  $t_{\text{crit},2(n-1)}(0.95)$  are provided by standard statistical software.

Table 1 shows the results of significance testing for the difference in population mean duty,  $\bar{Q5}_1 - \bar{Q5}_2$ , between trains Tr<sub>1</sub> and Tr<sub>2</sub>, annually from 2015 to 2019. In percentage terms,  $\bar{Q5}_1$  exceeds  $\bar{Q5}_2$  by some 2.8% to 6.4%.

Year	2015	2016	2017	2018	2019
$\bar{Q5}_1 - \bar{Q5}_2$	2.45	3.82	5.53	3.95	3.89
$s_p$	2.46	2.49	1.93	2.42	3.73
$s_d$	0.0598	0.125	0.0324	0.0236	0.0364
$\nu = 2(n - 1)$	6752	1584	14182	42144	41944
$t_{\text{crit},\nu}(0.95)$	1.65	1.65	1.65	1.65	1.65
LCL	2.33	3.57	5.47	3.90	3.81

Table 1: Independent two-sample t-test for population mean difference  $\bar{Q5}_1 - \bar{Q5}_2$  per annum. Null hypothesis rejected for each year since LCL<sub>0</sub>. Note that the critical value  $t_{\text{crit},\nu}(0.95)$  at infinite sample size is adopted as a good approximation, since  $n > 1000$  throughout.

When there is evidence that the variance of the two samples is not equal, we can use the Welch's t-test (Welch 1947) as an alternative to the test above. For the current data, using the corresponding Welch test at  $\alpha = 0.05$ , the null hypothesis of equality of  $\bar{Q5}_1$  and  $\bar{Q5}_2$  was also rejected for each of the years 2015 to 2019; see Appendix B for details.

### 3.3. Regression and adjusted regression plots

For each of units U<sub>1</sub> and U<sub>2</sub> on trains Tr<sub>1</sub> and Tr<sub>2</sub> respectively in turn, we establish linear regression models for Q5 in terms of Q3, T3 and P4 of the form

$$Q5 = f(Q3, T3, P4) + \epsilon \quad (4)$$

for regression function  $f$ , where  $\epsilon$  is assumed to be a zero-mean Gaussian random variable with unknown standard deviation. Here, we assume that  $f$  takes the linear form

$$f(Q3, T3, P4) = a + b Q3 + c T3 + d P4 \quad (5)$$

for parameters  $a$ ,  $b$ ,  $c$  and  $d$  to be estimated. Following DuMouchel (1988), we then use adjusted response or adjusted regression plots to quantify the effects of individual treatment variables (more naturally referred to as covariates in a regression context) in regression models for Q5 in terms of Q3, T3 and P4, for each of trains Tr<sub>1</sub> and Tr<sub>2</sub>. In essence, these are generalisations of partial residual and augmented partial residual plots (Mallows 1986), useful for linear regression models with arbitrary power and interaction terms. The fitted regression function  $\hat{f}$  from Equation 5 is

$$\hat{f}(Q3, T3, P4) = \hat{a} + \hat{b} Q3 + \hat{c} T3 + \hat{d} P4 \quad (6)$$

where  $\hat{\bullet}$  represents an estimate. The corresponding residuals from the regression form the set  $\{r^i\}_{i=1}^n$ , with

$$r^i = Q5^i - \hat{f}(Q3^i, T3^i, P4^i) \quad \text{for } i = 1, 2, \dots, n \quad (7)$$

where  $\{Q3^i, T3^i, P4^i\}_{i=1}^n$  is the set of values of Q3, T3 and P4 in the data sample of filtered data for regression model fitting.

Next, adjusted fit functions are calculated for each of Q3, T3 and P4 in turn. For example in the case of Q3, the adjusted fit function is the average value of  $\hat{f}$ , expressed as a function of Q3, over all n observations in the data sample

$$g_{Q3}(q) = \frac{1}{n} \sum_{i=1}^n \hat{f}(q, T3^i, P4^i). \quad (8)$$

Similar adjusted fit functions can be derived for each covariate in each train in turn. Finally the set  $\{\tilde{Q}5_{Q3}^i\}_{i=1}^n$  of adjusted response values for Q5 with respect to Q3 is calculated using

$$\tilde{Q}5_{Q3}^i = g_{Q3}(Q3^i) + r^i \quad \text{for } i = 1, 2, \dots, n \quad (9)$$

where  $\{r^i\}_{i=1}^n$  are the residuals from the full regression (Equation 4). Similar sets of adjusted response values can be calculated for response Q5 with respect to each covariate in each train in turn.

Adjusted response values for Q5 with respect to each of Q3, T3 and P4 are shown in Figure 6, for train Tr<sub>1</sub> (blue) and Tr<sub>2</sub> (red). The anticipated directions of the trends of Q5 with covariates are seen in each case. However, despite the trains being nominally replicates, the magnitudes of gradients are larger for train Tr<sub>1</sub> regardless of covariate. Briefly, Q5 is more sensitive to changes in covariates for train Tr<sub>1</sub>. To achieve unit reduction in Q5, the reduction in

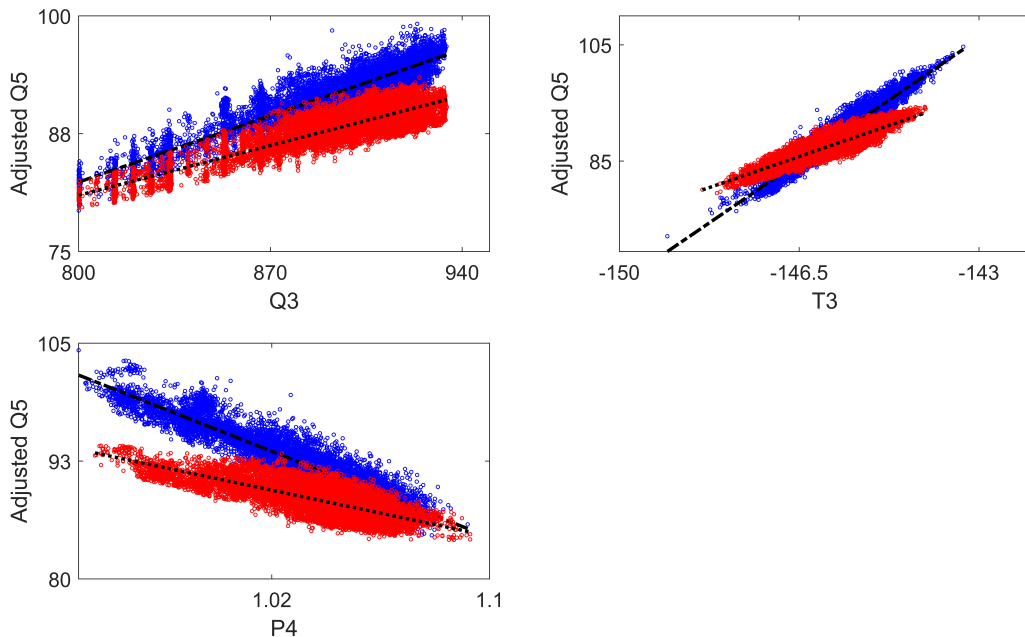


Figure 6: Adjusted response values for Q5 with respect to Q3, T3 and P4 for U<sub>1</sub> (blue circles) and U<sub>2</sub> (red circles). Corresponding adjusted fit functions  $g$  are shown as black lines

Q3 (and/or T3) needed in Tr<sub>1</sub> is smaller than that needed in Tr<sub>2</sub>. This is potentially a valuable handle with which to reduce the need for flaring.

Note that the adjusted regression methodology is applicable generally, regardless of the form of the regression function in Equation 4.

### 3.4. Implementation of recommendations

Given the findings above, trials were conducted on the liquefaction trains to evaluate the impact on flaring of different manipulations of set-points of manipulated variables on  $\text{Tr}_1$  and  $\text{Tr}_2$  end flash units  $U_1$  and  $U_2$ . In a first period (“Period 1”), each time the flare valve was on the verge of opening, a common reduction of  $T_3$  was made for both trains, followed by common reduction of  $Q_3$  if necessary. In the second period (“Period 2”), preferential treatment was given to  $\text{Tr}_1$ :  $T_{31}$  was reduced first, followed if necessary by  $Q_{31}$ ,  $T_{32}$  and  $Q_{32}$  if flaring persisted.  $P_4$  was not used as a handle during the trial. Results are shown in Figure 7. Panels show the mean flare valve opening

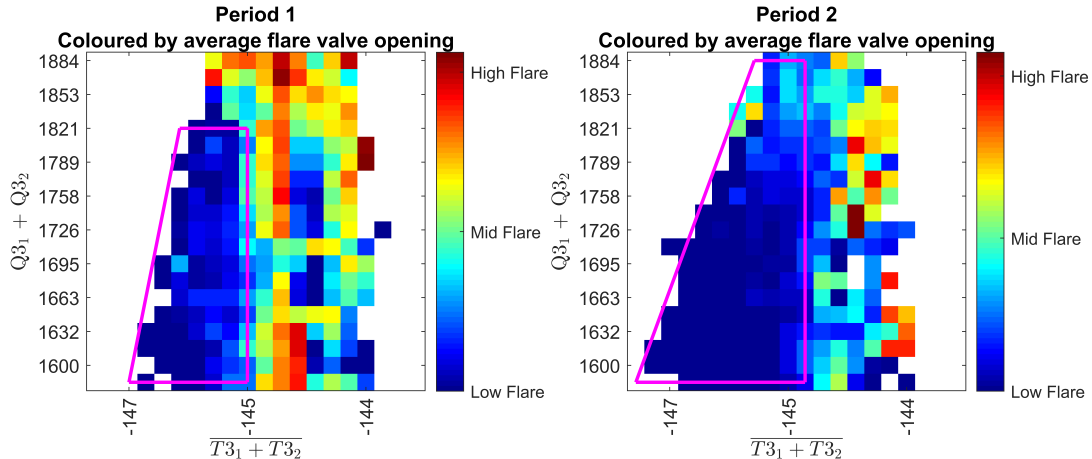


Figure 7: Flare valve opening, ranging from High, Medium to Low for Period 1 (left) and Period 2 (right) as a function of mean of  $T_3$  and sum of  $Q_3$  from  $\text{Tr}_1$  and  $\text{Tr}_2$ . In Period 1, simultaneous and equal reductions were made, first for  $T_3$  and subsequently if necessary for  $Q_3$ , for both trains at the point of flare onset. In Period 2,  $T_{31}$  and then  $Q_{31}$  (if necessary) were reduced first, followed (if necessary) by  $T_{32}$  and  $Q_{32}$ . Polygons shows domains of mean  $T_3$  and total  $Q_3$  corresponding to low risk of High and Medium flare opening

in Periods 1 (left) and 2 (right) as a function of the mean  $T_3$  (x-axis) and total  $Q_3$  (y-axis). The figure indicates a reduction in High and Medium flare valve opening in Period 2 compared to Period 1, resulting in a reduction of up to 45% in flaring-related CO<sub>2</sub> emissions. Polygons (magenta) in each panel show approximate ranges for mean  $T_3$  and total  $Q_3$  within which the risk of High or Medium flaring is low. The area of the polygon for Period 2 is considerably wider than for Period 1, indicating that reduction of  $T_3$  and  $Q_3$  for  $\text{Tr}_1$  before those of  $\text{Tr}_2$  is advantageous in reducing FG flaring.

## 4. Discussion and conclusions

This article demonstrates that differences in the operating characteristics of nominally replicate units at an LNG facility can be exploited to improve the overall performance of the facility, in particular by minimising flaring. We demonstrate that careful exploratory analysis can be used to identify differences in operating characteristics, and that statistical hypothesis testing lends weight to findings from exploratory work. We then show that simple regression models can be used to illustrate and quantify differences in unit performance. Finally, we demonstrate by modifying operating practices at the “live” LNG facility, that the recommendations of the statistical analysis provide clear material benefit. We emphasise that this paper exploits real operational data from the full-scale LNG facility.

The statistical analysis conducted here is elementary but sound. Indeed, we hope the current work demonstrates the real-world benefits available from careful application of straightforward statistical thinking and method: complicated models are not always necessary for process improvement in manufacturing. Nevertheless, there are numerous ways in which the current analysis can be improved. For example, preliminary analysis suggests there may be some benefit from consideration of seasonal trends in the relative operating characteristics of the flash vessel units.

Specifically, our study of end flash vessels from two trains at an LNG facility has shown that statistically significant differences in train performance can exist even though trains may be “exact copies” of each other from a design perspective. In fact, although the end flash vessels in the two trains are designed to identical specification, in operation they may not perform equivalently due to a number of reasons. For example, they may be exposed to different localised variation in ambient conditions, causing variation in end flash gas produced. We actually observe the flow rate of end flash gas (EFG, Q5) produced from one end flash vessel to be 2.8% to 6.4% higher than from the other replicate unit. As a result, on the onset of EFG flaring, the standard practice of reducing natural gas input temperature (T3) and flow rate (Q3) simultaneously and equally to the main cryogenic heat exchangers of the two trains to minimise flaring is demonstrably not best practice. An improved procedure based on the current statistical analysis first reduces T3 and Q3 for the train whose EFG production is more sensitive to operating conditions. When this strategy was followed at the LNG facility, flaring-related CO<sub>2</sub> emissions were reduced by up to 45% compared with standard practice, noting that flaring emissions for a typical LNG facility account for approximately 4% to 8% of the overall facility emissions.

Insights from analysis of operational data cannot be obtained from simulation studies of model trains with identical designs. We hope the current paper serves as motivation for wider use of data-informed and data-driven approaches for improved efficiency in manufacturing.

#### **Appendix A: Annual summary statistics for Q5 from trains Tr<sub>1</sub>, Tr<sub>2</sub> for years 2015-2019**

This appendix gives summary statistics for normalised filtered Q5 from trains Tr<sub>1</sub>, Tr<sub>2</sub> for years 2015-2019, corresponding to Figure 4. These values are also used in the statistical testing reported in Section 3.

Year	Mean	Median	Variance $s^2$	Skewness	Kurtosis
2015	89.34	89.80	7.22	-1.17	5.69
2016	90.78	91.15	8.30	-1.95	10.03
2017	90.78	91.15	4.13	-0.38	3.56
2018	92.77	93.13	6.84	-1.08	6.34
2019	91.90	92.99	20.08	-1.54	5.26

Table A1: Summary statistics of samples of filtered Q5 values for train Tr<sub>1</sub> over years 2015 to 2019. Values have been normalised using a common factor so that the global maximum value (over both trains and all years) is 100 T/d.

Year	Mean	Median	Variance	Skewness	Kurtosis
2015	86.89	87.02	4.86	-0.86	8.29
2016	86.96	86.58	4.09	0.15	2.67
2017	85.25	85.54	3.30	-0.91	4.34
2018	88.83	89.11	4.85	-0.87	4.91
2019	88.02	88.19	7.74	-1.28	6.93

Table A2: Summary statistics of filtered Q5 values for train Tr<sub>2</sub> over years 2015 to 2019. Values have been normalised using a common factor so that the global maximum value (over both trains and all years) is 100 T/d.

#### **Appendix B: One-tailed, two-sample Welch's t-test for un-equal variance**

In the notation of Section 3.2, the expression for Welch's t-test statistic (Welch 1947) to compare the means of populations with unequal population variances of  $X_1$  and  $X_2$ , but equal sample size  $n$ , is the same as that given in Equation 2. The degrees of freedom  $\nu$  of the t-distribution is however different, given by Satterthwaite's approximation (Satterthwaite, 1946) as

$$\nu = \frac{(n-1)(s_1^2 + s_2^2)^2}{s_1^4 + s_2^4} \quad (10)$$

where  $s_1$  and  $s_2$  are the corrected sample standard deviations for the two groups; the Welch's t-test is more conservative in estimating  $\nu$ . The corresponding table of results using Welch's t-test is given in Table (c.f. Table 1) is given in Table B1.

Year	2015	2016	2017	2018	2019
$\overline{Q5}_1 - \overline{Q5}_2$	2.45	3.82	5.53	3.95	3.89
$\nu$	6505	1420	14007	40953	35055
$t_{\text{crit},\nu}(0.95)$	1.96	1.96	1.96	1.96	1.96
LCL	2.33	3.57	5.47	3.90	3.81

Table B1: Welch's t-test for population mean difference  $\overline{Q5}_1 - \overline{Q5}_2$  per annum, assuming unequal population variances. Null hypothesis rejected for each year since  $\text{LCL}_i > 0$ . Note that the critical value  $t_{\text{crit},\nu}(0.95)$  at infinite sample size is adopted as a good approximation, since  $n > 1000$  throughout.

## References

- Alabdulkarem, A., Mortazavi, A., Hwang, Y., Radermacher, R., and Rogers, P. (2011). Current Status and Perspectives of Liquefied Natural Gas (LNG) Plant Design. *Applied Thermal Engineering*, 31:1091–1098.
- Ali, W., Qyyum, M. A., Qadeer, K., and Lee, M. (2018). Energy optimization for single mixed refrigerant natural gas liquefaction process using the metaheuristic vortex search algorithm. *Applied Thermal Engineering*, 129:782–791.
- Austbo, B., Lovseth, S. W., and Gundersen, T. (2014). Annotated bibliography - Use of optimization in LNG process design and operation. *Computers and Chemical Engineering*, 71:391–414.
- Bassioni, G. and Klein, H. (2024). Liquefaction of natural gas and simulated process optimization : A review. *Ain Shams Engineering Journal*, 15:102431.
- Castillo, L., Dahouk, M. M., Scipio, S. D., and Dorao, C. (2013). Conceptual analysis of the precooling stage for LNG processes. *Energy Conversion and Management*, 66:41–47.
- DuMouchel, W. (1988). Graphical representations of main effects and interaction effects in a polynomial regression on several predictors. In *DTIC ADA208838: Computing Science and Statistics: Proceedings of the 20th Symposium on the Interface: Computationally Intensive Methods in Statistics (Fairfax, Virginia)*, pages 127–132.
- Evans, M., Hastings, N., and Peacock, B. (2000). *Statistical Distributions*. Wiley.
- Ferrin, J. L. and Perez-Perez, L. J. (2020). Numerical simulation of natural convection and boil-off in a small size pressurized LNG storage tank. *Computers and Chemical Engineering*, 138:106840.
- Hafner, M. and Luciani, G., editors (2022). *The Palgrave Handbook of International Energy Economics*.
- Hasan, M., Karimi, I., and Alfadala, H. (2009a). Optimizing compressor operations in an LNG plant. *Proceedings of the 1st Annual Gas Processing Symposium*, 48:179–184.
- Hasan, M. M. F., Zheng, A. M., and Karimi, I. A. (2009b). Minimizing boil-off losses in liquefied natural gas transportation. *Ind. Eng. Chem. Res.*, 48:9571–9580.
- International Energy Agency (2019). The role of gas in today's energy transitions.
- International Energy Agency (2022). World energy outlook.
- Jackson, S., Eiksund, O., and Broda, E. (2017). Impact of ambient temperature on LNG liquefaction process performance: Energy efficiency and CO<sub>2</sub> emissions in cold climates. *Industrial and Engineering Chemical Research*, 56:3388–3398.
- Jin, C., Lim, Y., and Xu, X. (2023). Performance analysis of a boil-off gas re-liquefaction process for LNG carriers. *Energy*, 278:127823.
- Katebah, M. A., Hussein, M. M., Al-musleh, E. I., and Almomani, F. (2023). A systematic optimization approach of an actual LNG plant: Power savings and enhanced process economy. *Energy*, 269:126710.
- Kurle, Y. M., Wang, S., and Xu, Q. (2017). Dynamic simulation of LNG loading, BOG generation, and BOG recovery at LNG exporting terminals. *Computers and Chemical Engineering*, 97:47–58.
- Lim, W., Choi, K., and Moon, I. (2012). Current status and perspectives of liquefied natural gas (LNG) plant design. *Industrial and Engineering Chemistry Research*, 52:3056–3088.

- Mallows, C. L. (1986). Augmented partial residuals. *Technometrics*, 28:313–319.
- Marshall, G. and Jonker, L. (2011). An introduction to inferential statistics: A review and practical guide. *Radiography*, 17:1–6.
- Satterthwaite, F. (1946). An approximate distribution of estimates of variance components. *Biometrics Bulletin*, 2:110–14.
- Shin, K., Son, S., Moon, J., Jo, Y., Kwon, J. S., and Hwang, S. (2022). Dynamic modeling and predictive control of boil-off gas generation during LNG loading. *Computers and Chemical Engineering*, 160:107698.
- Welch, B. L. (1947). The generalisation of “student’s” problem when several different population variances are involved. *Biometrika*, 34:28–35.
- Widodo, A. and Muharam, Y. (2023). Simulation of boil-off gas recovery and fuel gas optimization for increasing liquefied natural gas production. *Energy Reports*, 10:4503–4515.
- Wu, S. and Ju, Y. (2021). Numerical study of the boil-off gas (BOG) generation characteristics in a type C independent liquefied natural gas (LNG) tank under sloshing excitation. *Energy*, 223:120001.